Supporting Information

Rational construction of self-supported triangle-like MOF-derived hollow $(Ni,Co)Se_2$ arrays for electrocatalysis and supercapacitor

Wenjiao Song,† Xue Teng,† Yangyang Liu,† Jianying Wang,† Yanli Niu,† Xiaoming He,† Cheng Zhang‡ and Zuofeng Chen*,†

†Shanghai Key Laboratory of Chemical Assessment and Sustainability, School of Chemical Science and Engineering, Tongji University, Shanghai 200092, China;

‡College of Chemical Engineering and Materials Science, Zhejiang University of Technology, Hangzhou 310014, China

EXPERIMENTAL

Chemicals. Cobalt nitrate hexahydrate ($Co(NO_3)_2·6H_2O$, 98%), nickel nitrate hexahydrate ($Ni(NO_3)_2·6H_2O$, 98%), 2-methylimidazole ($C_4H_6N_2$, 98%), sodium borohydride ($NaBH_4$, 96%), selenium (Se, 99.9%), potassium hydroxide (KOH, 99%), acetone (C_3H_6O, 99.5%) and ethanol (C_2H_5OH, 99.5%) were obtained from Sigma Aldrich. The carbon cloth was obtained from Shanghai Hesen Electric Co. (HCP330N, 32 cm × 16 cm, 0.32 mm). All reagents were analytical grade and used as received without further purification. Deionized water (18.0 MΩ cm) was used for preparing electrolyte solutions in all experiments.

Procedures. *Preparation of MOF-Co/CC.* Before being used, the carbon cloth

(CC) was cleaned with acetone, ethanol and distilled water under ultrasonication. The MOF-Co/CC electrode was synthesized according to the following procedure. Briefly, a certain volume of pre-prepared 2-methylimidazole aqueous solution (0.4 M) was quickly added into the same volume aqueous solution of $Co(NO_3)_2 \cdot 6H_2O$ (50 mM). After being mixed under magnetic stirring for 1 min, a piece of clean CC substrate was immersed into the obtained mixture and maintained at room temperature for 4 h. Then the electrode was taken out, cleaned with distilled water and ethanol for several times and finally dried at 60 °C in an electric oven to get the purple MOF-Co/CC product.

Preparation of NiCo-LDH/CC. A piece of MOF-Co/CC was immersed into an ethanol solution (30 mL) containing $Ni(NO_3)_2 \cdot 6H_2O$ (0.09 g) and kept still at room temperature for 2 h. After the reaction, the obtained light green electrode was washed with distilled water and ethanol for several times and dried at 60 °C.

Preparation of (Ni,Co)Se_2/CC. Before the selenization, NaHSe solution was synthesized. In a typical procedure, 0.065 g $NaBH_4$ was dissolved into 1.5 mL deionized water under N_2 flow to achieve a clear solution, after which 0.059 g Se powder was added into the pre-prepared $NaBH_4$ aqueous solution. The mixture was thoroughly mixed under N_2 flow to obtain the clear NaHSe solution. The as-prepared NiCo-LDH/CC was transformed into (Ni,Co)Se_2/CC by a solvothermal selenization. The freshly made NaHSe solution was added into 30 mL N_2-saturated ethanol, and the flow of N_2 was maintained during the whole process. Then the mixed solution was transferred into 50 mL Teflon-lined stainless steel autoclave followed by the

immersion of a piece of NiCo-LDH/CC. The (Ni,Co)Se_2/CC was finally obtained after being heated in an electric oven at 140 °C for 10 h.

Preparation of $CoSe_2$/CC. Following the preparation of the MOF-Co/CC array electrode, the $Co(OH)_2$/CC array electrode was first synthesized via a similar ion-etching process by replacing $Ni(NO_3)_2$ with $Co(NO_3)_2$ and then transformed into $CoSe_2$ by the same selenization procedure.

Apparatus. X-ray diffraction (XRD) measurements were performed on Bruker Foucs D8 via ceramic monochromatized Cu Kα radiation of 1.54178 Å, with the operating voltage of 40 kV and current of 40 mA.

Scanning electron microscopy (SEM) images were acquired by using a Hitachi S-4800 (Hitachi, Japan) microscope equipped with an energy-dispersive X-ray spectroscopy (EDS) instrumentation, and the operating voltage for SEM imaging and EDX analysis and mapping were 3 kV at 15 kV, respectively. Transmission electron microscopy (TEM) measurements were carried out on a JEM-2100, JEOL microscope.

X-ray photoelectron spectroscopy (XPS) was recorded through a Kratos Axis Ultra DLD X-ray Photoelectron Spectrometer. The XPS binding energies were calibrated using the C 1s level of 284.6 eV, which was taken as a reference.

The electrochemical performance of the samples toward oxygen evolution reaction (OER) and as a supercapacitor electrode were tested at room temperature in a three-electrode configuration on an electrochemical workstation (CHI660E), with the synthesized materials, Hg/HgO/1 M KOH electrode and Pt plate selected as the working electrode, reference electrode and counter electrode, respectively.

For OER test, the whole measurement process was conducted in 1 M KOH electrolyte. All potentials reported in this work were calculated with respect to the reversible hydrogen electrode (RHE) using the following equation: E(RHE) = E(Hg/HgO) + 0.059 pH + 0.098 V. Prior to the test, the electrodes were activated by cyclic voltammetry scanning at a scan rate of 10 mV s^{-1}. Linear sweep voltammetry was performed at 5 mV s^{-1} in the potential range from 0.14 to 0.94 V (vs. Hg/HgO). Tafel slopes for evaluating the OER kinetics of catalysts were acquired based on the polarization curves by plotting η vs. log current density (j). Electrochemical impedance spectroscopy (EIS) measurements were carried out under a given overpotential over the frequency range 0.01 Hz to 100 kHz. The electrochemical surface area (ESCA) of the catalysts was assessed by double-layer capacitance (C_{dl}), which can be determined using simple CV measurements. The CV measurements were performed in a potential window with non-Faradaic processes at various scan rates. By plotting the capacitive current density at a specific potential versus scan rate, the slope of the fitted linear curve yielded the C_{dl} value.

Electrochemical supercapacitor measurements were carried out using a three-electrode setup with 6 M KOH aqueous solution as the electrolyte. The CV curves were recorded in a potential range of 0 - 0.6 V (vs. Hg/HgO) at various scan rates. The galvanostatic charge-discharge (GCD) curves at different current densities were collected and used for calculating the specific capacitance of the materials based on the equations $C = I\,\Delta t/\Delta V$, where I is the GCD current density, Δt is the discharge time, and ΔV is the potential window. EIS was measured under the similar parameter

settings as OER.

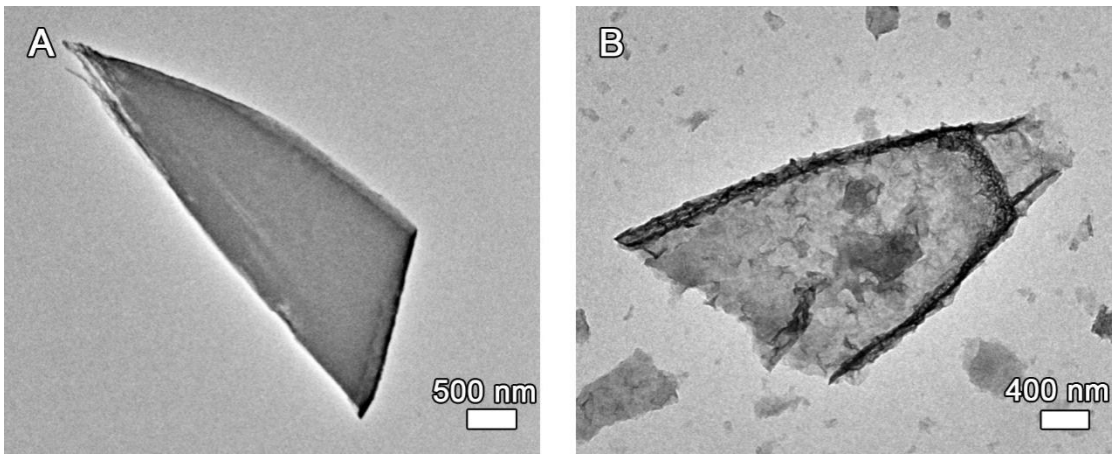

Figure S1. TEM images of (A) MOF-Co and (B) NiCo-LDH.

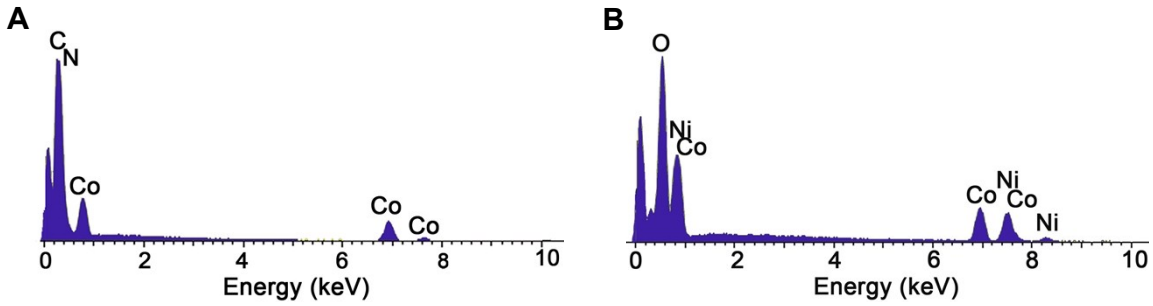

Figure S2. The EDX results of (A) MOF-Co and (B) NiCo-LDH.

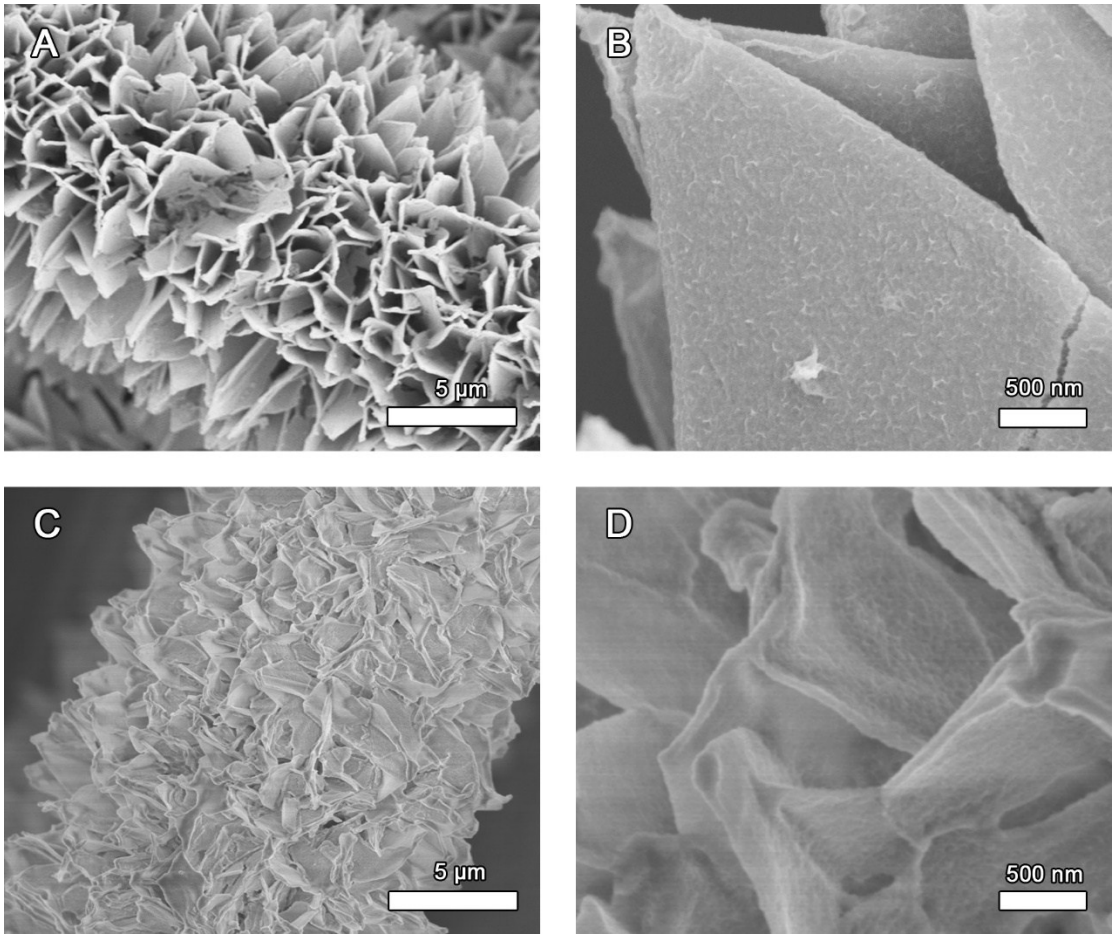

Figure S3. SEM images showing (A,B) insufficient etching with 1 h reaction time. (C,D) Destruction of the arrays due to the excessive etching of MOF-Co when the ion-exchange reaction is extended to 3 h.

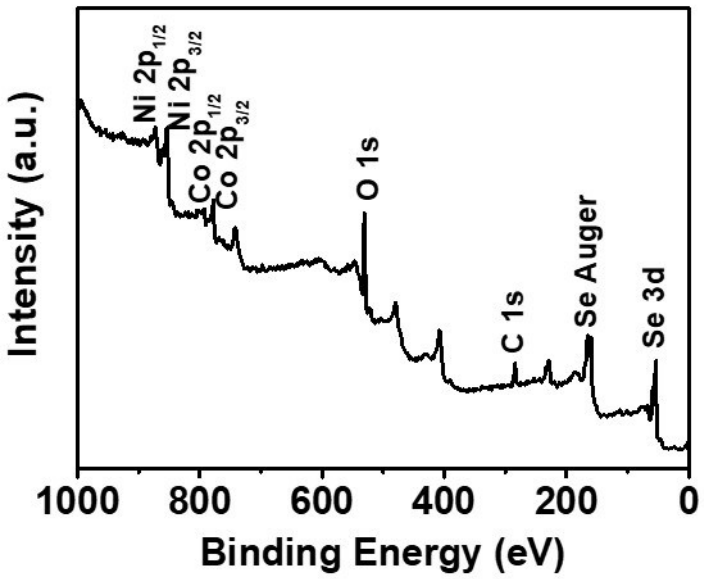

Figure S4. XPS survey spectrum of (Ni,Co)Se_2/CC.

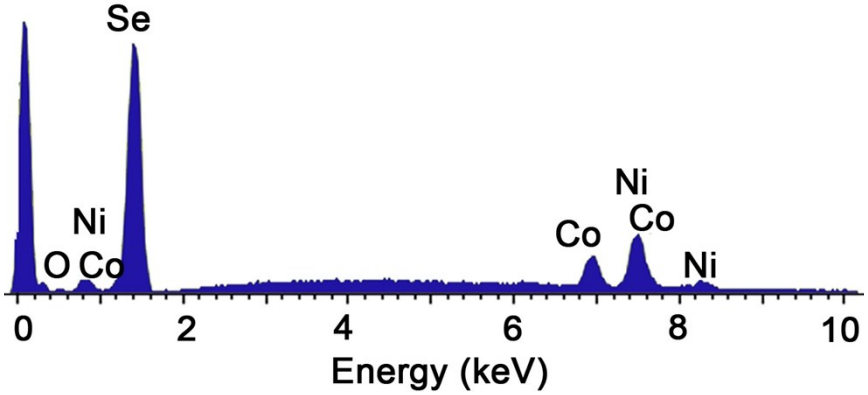

Figure S5. EDX result of (Ni,Co)Se_2/CC.

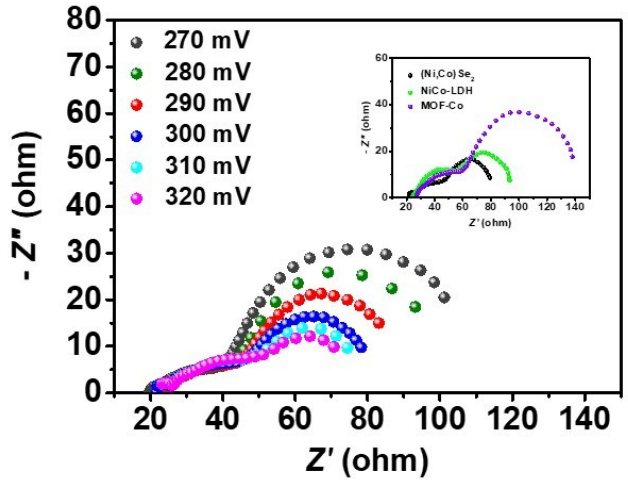

Figure S6. Nyquist plots for $(Ni,Co)Se_2$ at various overpotentials. Inset shows the Nyquist plots of $(Ni,Co)Se_2$, NiCo-LDH and MOF-Co at a constant overpotential of 300 mV.

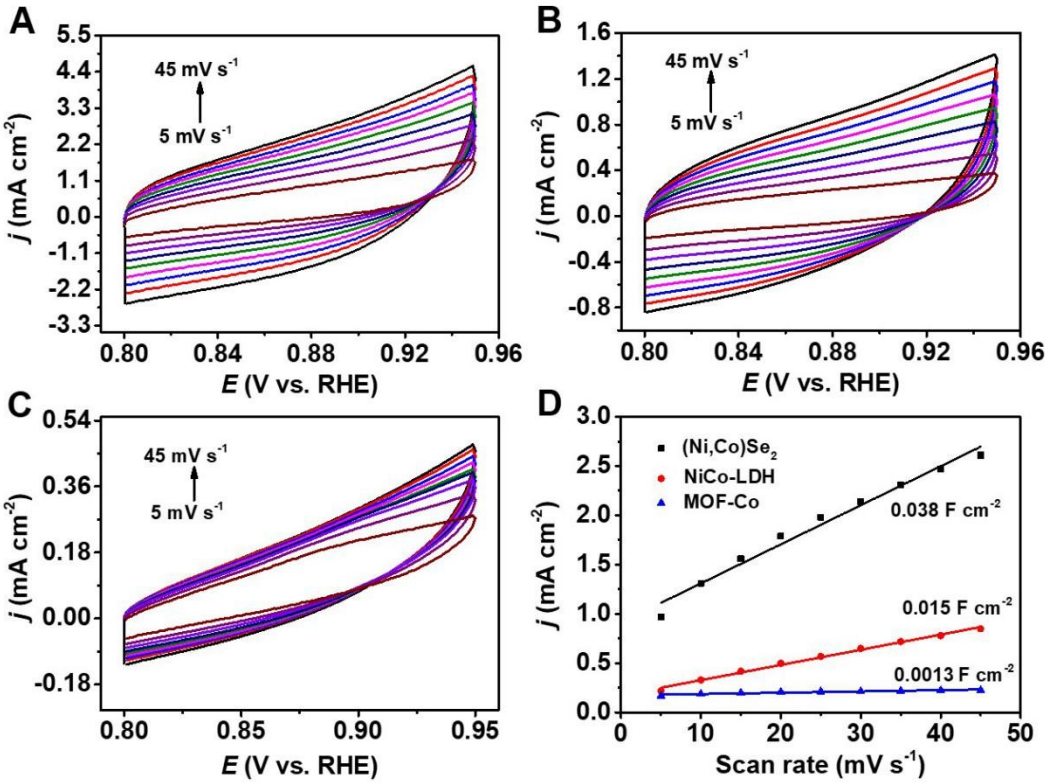

Figure S7. Measurements of the electrochemically active surface areas of the electrode samples: cyclic voltammograms at different scan rates for (A)

(Ni,Co)Se_2/CC, (B) NiCo-LDH/CC, and (C) MOF-Co/CC. (D) Plots of the scan rate versus the current density at 0.88 V vs. RHE.

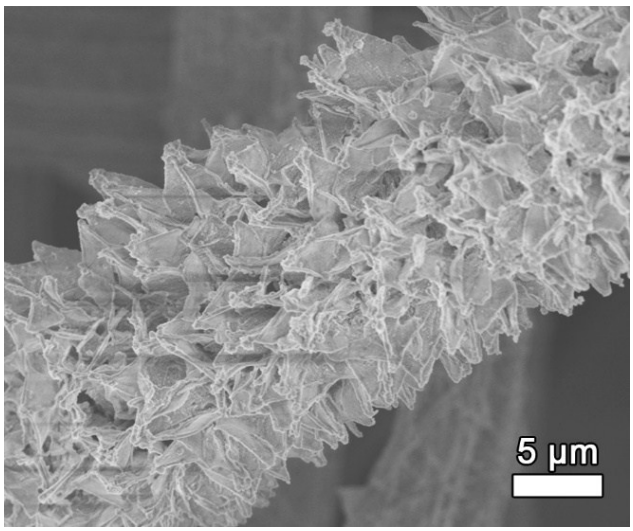

Figure S8. SEM image of (Ni,Co)Se_2/CC after OER test.

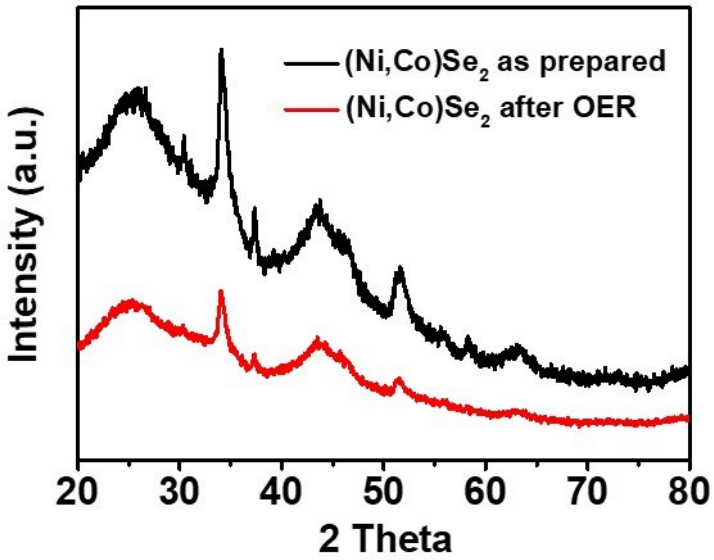

Figure S9. XRD patterns of the (Ni,Co)Se_2/CC before and after OER test.

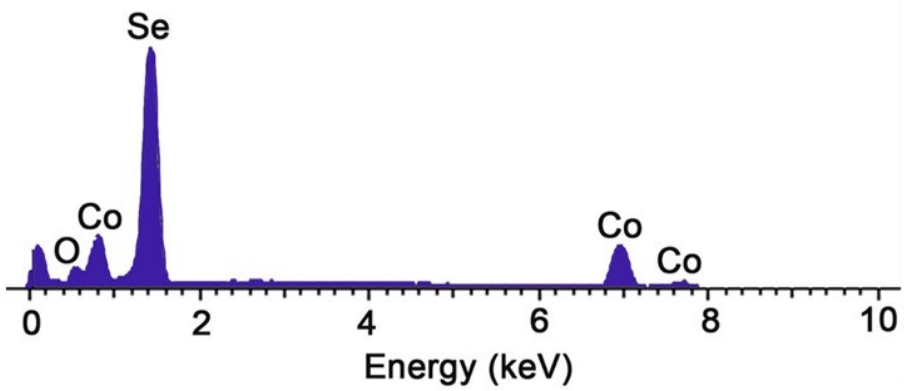

Figure S10. EDX result of $CoSe_2$/CC.

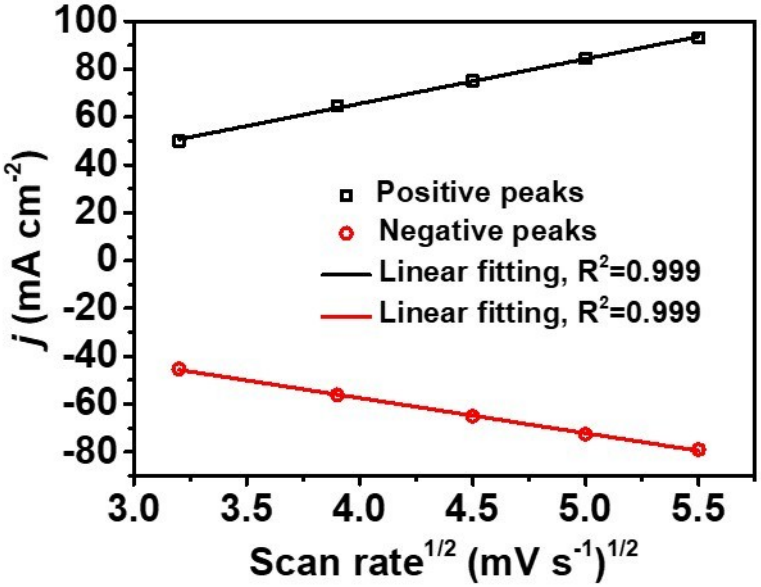

Figure S11. Plots of corresponding anodic and cathodic peak current densities presented in Figure 5A versus the square root of scan rate.

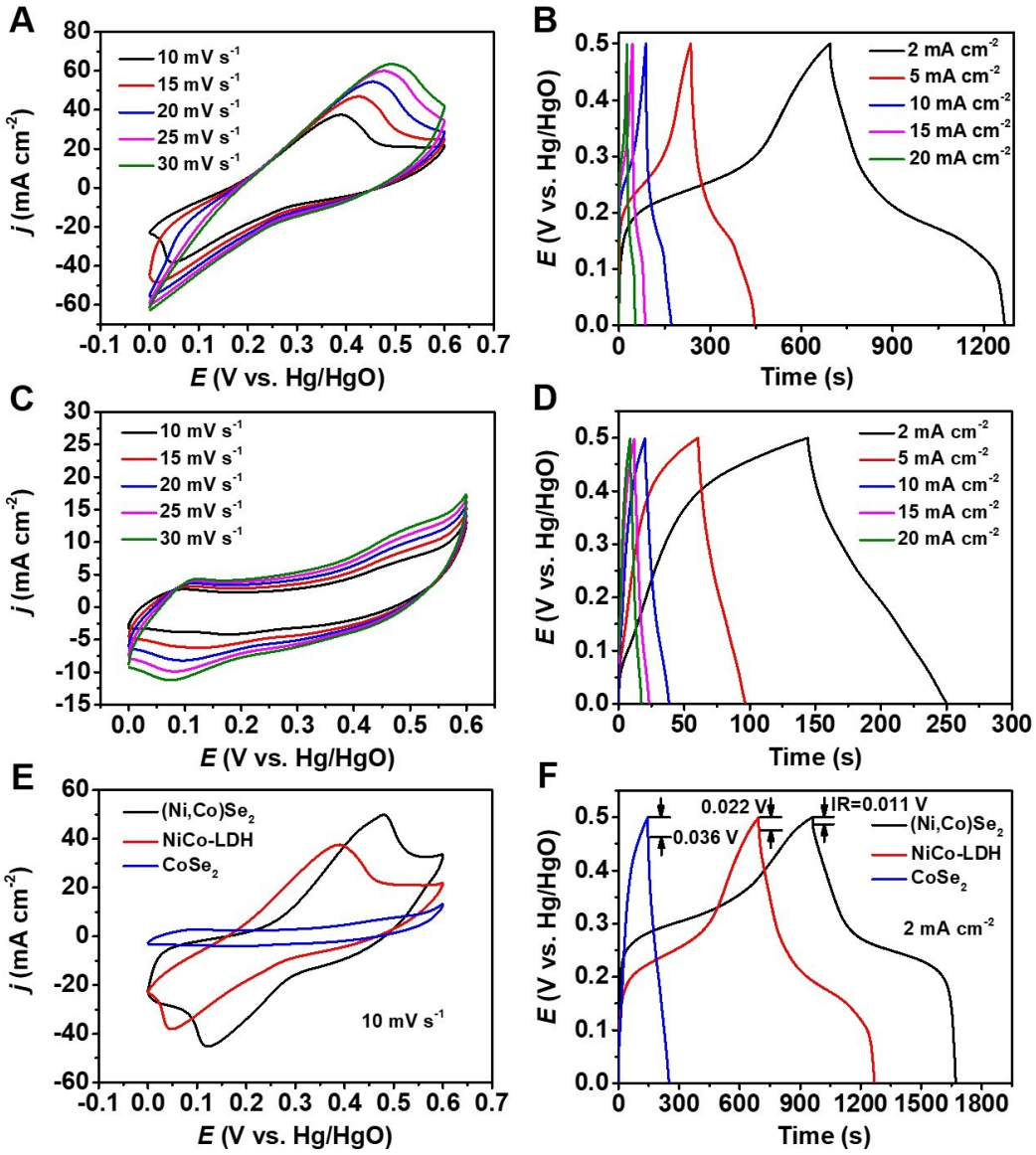

Figure S12. (A) CV curves and (B) GCD curves of NiCo-LDH/CC; (C) CV curves and (D) GCD curves of $CoSe_2$/CC. (E) CV curves at 10 mV s^{-1} and (F) GCD curves at 2 mA cm^{-2} for (Ni,Co)Se_2/CC, NiCo-LDH/CC and $CoSe_2$/CC.

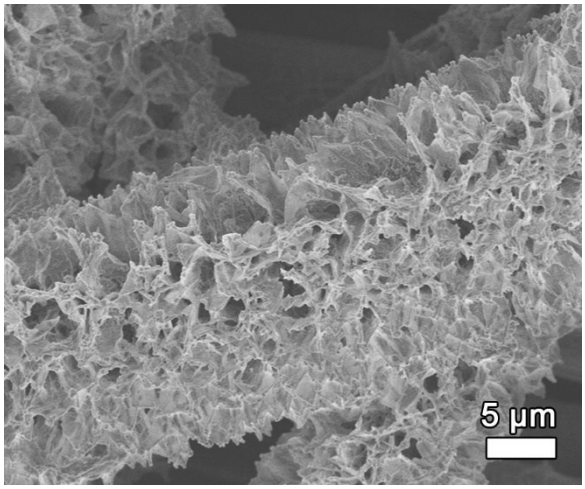

Figure S13. SEM image of (Ni,Co)Se_2/CC after 2000 charge-discharge cycles.

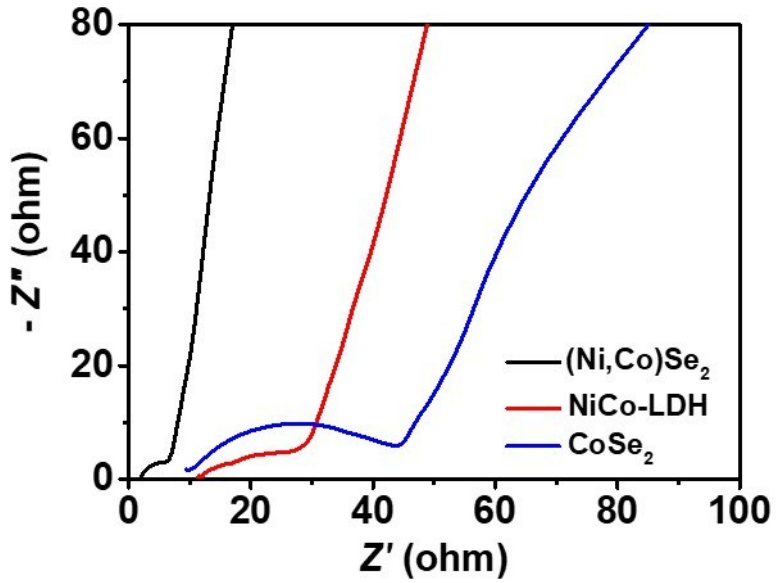

Figure S14. EIS plots of (Ni,Co)Se_2, NiCo-LDH and $CoSe_2$ tested at an open circuit potential.

Table S1. Comparison of electrochemical OER performance of $(Ni,Co)Se_2$/CC and other selenides catalysts in 1 M KOH solution.

Catalysts	Substrate	Current density ($mA\ cm^{-2}$)	Overpotential (mV)	Tafel slope ($mV\ dec^{-1}$)	Ref.
$(Ni, Co)_{0.85}Se$ nanotubes	Carbon Cloth	10	255	79	1
$NiSe_2$ nanowrinkles	Ni foam	100	337	63	2
$CoSe_2$ nanoparticles	Carbon cloth	10	297	41	3
$(Ni,Co)_{0.85}Se$ nanosheets	Ni foam	20	287	87	4
Co-Ni-Se/C	Ni foam	30	275	63	5
Co-doped $NiSe_2$ nanoparticles film	Ti plate	100	320	94	6
$CoNiSe_2$ nanorods	Ni foam	100	307	79	7
$NiCoSe_2$ nanobrush	Ni foam	10	274	61	8
Hollow $(Ni,Co)Se_2$ arrays	**Carbon cloth**	**10**	**256**	**74**	**This work**

Table S2. Comparison of electrochemical performance of $(Ni,Co)Se_2$/CC and other selenides electrodes for supercapacitors.

Electrode	Substrate	Electrolyte (KOH)	Current density	Specific Capacitance	Ref.
$(Ni,Co)_{0.85}Se$	Carbon fabric	1 M	4 mA cm^{-2}	2.33 F cm^{-2}	9
Hollow core-branch $CoSe_2$	Carbon cloth	3 M	1 mA cm^{-2}	759.5 F g^{-1}	10
NiSe nanorods	Nickel foam	6 M	5 mA cm^{-2}	6.81 F cm^{-2}	11
$Ni_{0.85}Se$ nanosheets	Nickel foam	3 M	1 A g^{-1}	3105 F g^{-1}	12
Ni-Co selenide nanorods	Nickel foam	1 M	4 mA cm^{-2}	2.61 F cm^{-2}	13
Porous $CoSe_2$ nanosheets	Carbon cloth	3 M	1 mA cm^{-2}	713.9 F g^{-1}	14
Bamboo like $CoSe_2$ arrays	Carbon cloth	3 M	1 mA cm^{-2}	544.6 F g^{-1}	15
Hollow $(Ni,Co)Se_2$ arrays	**Carbon cloth**	**6 M**	**2 mA cm^{-2}**	**2.85 F cm^{-2}**	**This work**

Supplementary References

1. C. Xia, Q. Jiang, C. Zhao, M. N. Hedhili and H. N. Alshareef, *Adv. Mater.*,

2016, **28**, 77-85.

2. J. Zhang, Y. Wang, C. Zhang, H. Gao, L. Lv, L. Han and Z. Zhang, *ACS Sustain. Chem. Eng.*, 2018, **6**, 2231-2239.

3. C. Sun, Q. Dong, J. Yang, Z. Dai, J. Lin, P. Chen, W. Huang and X. Dong, *Nano Res.*, 2016, **9**, 2234-2243.

4. K. Xiao, L. Zhou, M. Shao and M. Wei, *J. Mater. Chem. A*, 2018, **6**, 7585-7591.

5. F. Ming, H. Liang, H. Shi, X. Xu, G. Mei and Z. Wang, *J. Mater. Chem. A*, 2016, **4**, 15148-15155.

6. T. Liu, A. M. Asiri and X. Sun, *Nanoscale*, 2016, **8**, 3911-3915.

7. T. Chen and Y. Tan, *Nano Res.*, 2018, **11**, 1331-1344.

8. H. Zhu, R. Jiang, X. Chen, Y. Chen and L. Wang, *Sci. Bull.*, 2017, **62**, 1373-1379.

9. C. Xia, Q. Jiang, C. Zhao, P. M. Beaujuge and H. N. Alshareef, *Nano Energy*, 2016, **24**, 78-86.

10. T. Chen, S. Li, J. Wen, P. Gui, Y. Guo, C. Guan, J. Liu and G. Fang, *Small*, 2017, **14**, 1700979.

11. Y. Tian, Y. Ruan, J. Zhang, Z. Yang, J. Jiang and C. Wang, *Electrochim. Acta*, 2017, **250**, 327-334.

12. L. Du, W. Du, H. Ren, N. Wang, Z. Yao, X. Shi, B. Zhang, J. Zai and X. Qian, *J. Mater. Chem. A*, 2017, **5**, 22527-22535.

13. P. Xu, W. Zeng, S. Luo, C. Ling, J. Xiao, A. Zhou, Y. Sun and K. Liao,

Electrochim. Acta, 2017, **241**, 41-49.

14. T. Chen, S. Li, J. Wen, P. Gui and G. Fang, *ACS Appl. Mater. Interfaces*, 2017, **9**, 35927-35935.

15. C. Tian, L. Songzhan, G. Pengbin, W. Jian, F. Xuemei and F. Guojia, *Nanotechnology*, 2018, **29**, 205401.